Progress In Electromagnetics Research, PIER 22, 315–335, 1999

ELECTROMAGNETIC WAVE INTERACTION OF CONDUCTING OBJECT WITH ROUGH SURFACE BY HYBRID SPM/MOM TECHNIQUE

Y. Zhang, Y. E. Yang, H. Braunisch, and J. A. Kong

Department of Electrical Engineering and Computer Science
Massachusetts Institute of Technology
Cambridge, MA 02139

1. INTRODUCTION

Recently, there has been a great interest in studying the electromagnetic wave scattering from an object situated above a rough surface [1–7]. Simulation techniques for electromagnetic wave scattering by arbitrarily shaped objects in free space are well developed using wire [8–10] and surface-patch models [11–18]. The theory and numerical approaches associated with objects near flat interfaces of layered media have also been studied extensively by many researchers [7, 19–30]. However, considering the interface to be a rough surface is a new challenge, and little work has been reported. In theory, the standard MoM can be used to solve for the unknowns both on the object and the rough surface [4, 28, 31]. However, the discretization of the rough surface sig-

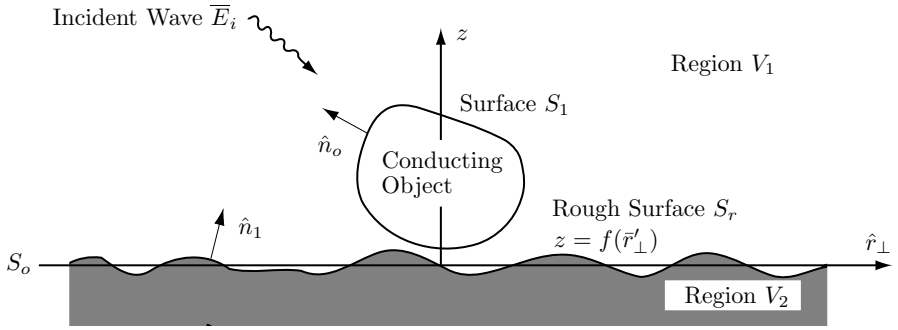

Figure 1. Configuration of the problem.

nificantly increases the computational resource requirements compared to calculating the scattering from the object alone. Therefore little literature exists on the study of scattering for full-scale geometry.

In this paper, we present a hybrid SPM/MoM technique to calculate the EM scattering from a 3-D conducting object above a rough surface. In this hybrid technique, the Green's function and surface variables are expanded in terms of the surface height function on the mean surface, and the electric integral equations based on the extinction theorem and the surface boundary conditions are decomposed into different orders. Each order represents a flat-surface scattering problem with the same geometry of the object and different equivalent sources, so that it can be solved efficiently by using the dyadic Green's function for layered media. The separation of the solution into different orders also helps us identify and characterize the individual interaction terms between the object and the rough surface.

2. CONFIGURATION AND FORMULATION

Consider an electromagnetic wave $\overline{E}_i(\bar{r})$ incident upon a perfectly conducting object with arbitrary shape S_1 above a rough surface S_r as shown in Fig. 1. The upper and lower spaces V_1 and V_2 are homogeneous and isotropic media characterized by (ϵ_1, μ_1) and (ϵ_2, μ_2), respectively. The rough surface profile is defined by the surface height function $f(\bar{r}'_\perp)$ with mean surface S_o coincident with the xy-plane.

2.1 Electric Field Integral Equations

On the perfectly conducting surface of the object, the tangential electric field is zero. Thus we can write the electric field integral equation for $\bar{r} \in S_1$ as

$$\left(\overline{E}_i(\bar{r}) + \iint_{S_r} dS' \left\{ i\omega\mu_1 \overline{\overline{G}}_1(\bar{r},\bar{r}') \cdot \left[\hat{n}_1(\bar{r}') \times \overline{H}_1(\bar{r}') \right] \right. \right.$$
$$\left. + \nabla \times \overline{\overline{G}}_1(\bar{r},\bar{r}') \cdot \left[\hat{n}_1(\bar{r}') \times \overline{E}_1(\bar{r}') \right] \right\}$$
$$\left. + i\omega\mu_1 \iint_{S_1} dS' \, \overline{\overline{G}}_1(\bar{r},\bar{r}') \cdot \overline{J}_1(\bar{r}') \right) \times \hat{n}_o(\bar{r}) = 0. \tag{1}$$

By applying the extinction theorem, we get for $\bar{r} \in V_2$

$$\overline{E}_i(\bar{r}) + \iint_{S_r} dS' \left\{ i\omega\mu_1 \overline{\overline{G}}_1(\bar{r},\bar{r}') \cdot \left[\hat{n}_1(\bar{r}') \times \overline{H}_1(\bar{r}') \right] \right.$$
$$\left. + \nabla \times \overline{\overline{G}}_1(\bar{r},\bar{r}') \cdot \left[\hat{n}_1(\bar{r}') \times \overline{E}_1(\bar{r}') \right] \right\}$$
$$+ i\omega\mu_1 \iint_{S_1} dS' \, \overline{\overline{G}}_1(\bar{r},\bar{r}') \cdot \overline{J}_1(\bar{r}') = 0, \tag{2}$$

and for $\bar{r} \in V_1$

$$\iint_{S_r} dS' \left\{ i\omega\mu_2 \overline{\overline{G}}_2(\bar{r},\bar{r}') \cdot \left[\hat{n}_2(\bar{r}') \times \overline{H}_2(\bar{r}') \right] \right.$$
$$\left. + \nabla \times \overline{\overline{G}}_2(\bar{r},\bar{r}') \cdot \left[\hat{n}_2(\bar{r}') \times \overline{E}_2(\bar{r}') \right] \right\} = 0, \tag{3}$$

where $\overline{\overline{G}}_1$ and $\overline{\overline{G}}_2$ are dyadic Green functions for unbounded regions with (ϵ_1, μ_1) and (ϵ_2, μ_2), respectively. The vector $\hat{n}_1(\bar{r}')$ denotes a local normal pointing from the rough surface S_r to the upper region V_1. The vector $\hat{n}_2(\bar{r}')$ is anti-parallel to $\hat{n}_1(\bar{r}')$, i.e., $\hat{n}_2(\bar{r}') = -\hat{n}_1(\bar{r}')$. $\overline{E}_1(\bar{r}')$ and $\overline{H}_1(\bar{r}')$ are electric and magnetic fields on the rough surface in region V_1, while $\overline{E}_2(\bar{r}')$ and $\overline{H}_2(\bar{r}')$ are surface fields on S_r in region V_2. $\overline{J}_1(\bar{r}')$ is the induced surface current on the object. If region V_2 is dielectric, the tangential fields are continuous, thus

$$\hat{n}_1(\bar{r}') \times \overline{H}_1(\bar{r}') = \hat{n}_1(\bar{r}') \times \overline{H}_2(\bar{r}') \equiv \frac{d\bar{r}'_\perp}{dS'\eta_1} \bar{a}(\bar{r}'_\perp), \tag{4}$$

$$\hat{n}_1(\bar{r}') \times \overline{E}_1(\bar{r}') = \hat{n}_1(\bar{r}') \times \overline{E}_2(\bar{r}') \equiv \frac{d\bar{r}'_\perp}{dS'} \bar{b}(\bar{r}'_\perp), \tag{5}$$

where $\bar{a}(\bar{r}'_\perp)$ and $\bar{b}(\bar{r}'_\perp)$ are new surface variables defined on the mean surface S_o, η_1 is the characteristic impedance of the upper region V_1, i.e., $\eta_1 = (\mu_1/\epsilon_1)^{1/2}$, and $d\bar{r}'_\perp$ is the projection of the infinitesimal area dS' on the mean surface S_o. With the new surface variables, we can rewrite the integral equations as

$$\left(\overline{E}_i(\bar{r}) + \iint_{S_o} d\bar{r}'_\perp \left\{ ik_1 \overline{\overline{G}}_1\left(\bar{r},\bar{r}'\right)\cdot\bar{a}(\bar{r}'_\perp) + \nabla\times\overline{\overline{G}}_1\left(\bar{r},\bar{r}'\right)\cdot\bar{b}(\bar{r}'_\perp)\right\} + i\omega\mu_1 \iint_{S_1} dS' \overline{\overline{G}}_1(\bar{r},\bar{r}')\cdot\overline{J}_1(\bar{r}')\right)\times\hat{n}_o(\bar{r}) = 0 \quad \text{for } \bar{r}\in S_1, \tag{6}$$

$$\overline{E}_i(\bar{r}) + \iint_{S_o} d\bar{r}'_\perp \left\{ ik_1 \overline{\overline{G}}_1\left(\bar{r},\bar{r}'\right)\cdot\bar{a}(\bar{r}'_\perp) + \nabla\times\overline{\overline{G}}_1\left(\bar{r},\bar{r}'\right)\cdot\bar{b}(\bar{r}'_\perp)\right\} + i\omega\mu_1 \iint_{S_1} dS' \overline{\overline{G}}_1(\bar{r},\bar{r}')\cdot\overline{J}_1(\bar{r}') = 0 \qquad \text{for } \bar{r}\in V_2, \tag{7}$$

$$\iint_{S_o} d\bar{r}'_\perp \left\{ ik_2\frac{\eta_2}{\eta_1}\overline{\overline{G}}_2\left(\bar{r},\bar{r}'\right)\cdot\bar{a}(\bar{r}'_\perp) + \nabla\times\overline{\overline{G}}_2(\bar{r},\bar{r}')\cdot\bar{b}(\bar{r}'_\perp)\right\} = 0 \qquad \text{for } \bar{r}\in V_1. \tag{8}$$

Theoretically, given the rough surface S_r and the object surface profile S_1, the unknown surface variables $\bar{a}(\bar{r}'_\perp)$, $\bar{b}(\bar{r}'_\perp)$ and the induced current $\overline{J}_1(\bar{r}')$ can be solved from Eqs. (6)–(8). For the special case in which the interface is flat, the surface variables $\bar{a}(\bar{r}'_\perp)$ and $\bar{b}(\bar{r}'_\perp)$ only have horizontal components, and the local coordinate $\bar{r}'$ in the dyadic Green functions $\overline{\overline{G}}_1(\bar{r},\bar{r}')$ and $\overline{\overline{G}}_2(\bar{r},\bar{r}')$ can be replaced by $\bar{r}'_\perp$.

2.2 Expansion of Green's Function and Surface Variables

We assume that the rough surface height is small. Therefore the scalar Green's function g_α in region V_α (where $\alpha = 1, 2$) can be expanded in terms of the surface height function $f(\bar{r}'_\perp)$ on the mean surface S_o,

$$\begin{aligned} g_\alpha(\bar{r},\bar{r}') &= g_\alpha\left(\bar{r},\bar{r}'_\perp + \hat{z}f(\bar{r}'_\perp)\right) \\ &= \sum_{m=0}^{\infty}\frac{1}{m!}\frac{\partial^m}{\partial z'^m} g_\alpha\left(\bar{r},\bar{r}'_\perp\right) f^m(\bar{r}'_\perp) \\ &= \sum_{m=0}^{\infty}\frac{1}{m!}\frac{\partial^m}{\partial z^m} g_\alpha\left(\bar{r},\bar{r}'_\perp\right)\left(-f(\bar{r}'_\perp)\right)^m, \end{aligned} \tag{9}$$

in which the following property of the scalar Green's function has been used:

$$\frac{\partial^m}{\partial z'^m} g_\alpha\left(\bar{r},\bar{r}'\right) = (-1)^m \frac{\partial^m}{\partial z^m} g_\alpha\left(\bar{r},\bar{r}'\right). \tag{10}$$

Thus the dyadic Green's function can be expressed as

$$\begin{aligned}\overline{\overline{G}}_\alpha(\bar{r},\bar{r}') &= \left(\overline{\overline{I}} + \frac{1}{k_\alpha^2}\nabla\nabla\right) g_\alpha(\bar{r},\bar{r}') \\ &= \sum_{m=0}^{\infty} \frac{1}{m!}\left(-f(\bar{r}'_\perp)\right)^m \frac{\partial^m}{\partial z^m}\overline{\overline{G}}_\alpha\left(\bar{r},\bar{r}'_\perp\right). \end{aligned}\tag{11}$$

Similarly, the surface variables and induced current can be written as series expansions as follows:

$$\overline{J}_1(\bar{r}') = \sum_{m=0}^{\infty} \overline{J}_1^{(m)}(\bar{r}'), \tag{12}$$

$$\bar{a}(\bar{r}'_\perp) = \sum_{m=0}^{\infty}\left[\bar{a}_\perp^{(m)}(\bar{r}'_\perp) + \hat{z}a_z^{(m)}(\bar{r}'_\perp)\right], \tag{13}$$

$$\bar{b}(\bar{r}'_\perp) = \sum_{m=0}^{\infty}\left[\bar{b}_\perp^{(m)}(\bar{r}'_\perp) + \hat{z}b_z^{(m)}(\bar{r}'_\perp)\right]. \tag{14}$$

In Eqs. (13) and (14), the separation of the z-components for the surface variables $\bar{a}$ and $\bar{b}$ allows the only unknown surface variables to become the tangential components since the z-components of the m-th order can be expressed in terms of the tangential components of order $(m-1)$, as we will see below. By the definition of $\bar{a}$ and $\bar{b}$ [Eqs. (4) and (5)], the following identities hold:

$$\hat{n}_1(\bar{r}'_\perp)\cdot\bar{a}(\bar{r}'_\perp) = 0, \tag{15}$$

$$\hat{n}_1(\bar{r}'_\perp)\cdot\bar{b}(\bar{r}'_\perp) = 0, \tag{16}$$

where

$$\hat{n}_1(\bar{r}'_\perp) = \frac{-\nabla'_\perp f(\bar{r}'_\perp) + \hat{z}}{\left|-\nabla'_\perp f(\bar{r}'_\perp) + \hat{z}\right|}. \tag{17}$$

Substituting the series expansions of $\bar{a}$ and $\bar{b}$, Eqs. (13) and (14), into Eqs. (15) and (16), respectively, and assuming that $\partial f(\bar{r}'_\perp)/\partial x'$ and $\partial f(\bar{r}'_\perp)/\partial y'$ are of the same order as $k_1 f(\bar{r}'_\perp)$, we then get the m-th

order z-components of the surface variables $\bar{a}$ and $\bar{b}$ in terms of their $(m-1)$-th order tangential components:

$$a_z^{(m)}(\bar{r}'_\perp) = \nabla'_\perp f(\bar{r}'_\perp) \cdot \bar{a}_\perp^{(m-1)}(\bar{r}'_\perp), \tag{18}$$

$$b_z^{(m)}(\bar{r}'_\perp) = \nabla'_\perp f(\bar{r}'_\perp) \cdot \bar{b}_\perp^{(m-1)}(\bar{r}'_\perp). \tag{19}$$

2.3 The n-th Order Equations

Substituting the series expansion for the dyadic Green's function Eq. (11) and the surface variables $\bar{a}$ and $\bar{b}$ as in Eqs. (13) and (14) into the integral equations (6)–(8), we can derive the following n-th order equations in terms of the surface height function $f(\bar{r}'_\perp)$:

$$\left(\overline{E}_i^{(n)}(\bar{r}) + \iint_{S_o} d\bar{r}'_\perp \left\{ ik_1 \overline{\overline{G}}_1\left(\bar{r}, \bar{r}'_\perp\right) \cdot \bar{a}_\perp^{(n)}(\bar{r}'_\perp) + \nabla \times \overline{\overline{G}}_1\left(\bar{r}, \bar{r}'_\perp\right) \cdot \bar{b}_\perp^{(n)}(\bar{r}'_\perp) \right\} + i\omega\mu_1 \iint_{S_1} dS' \overline{\overline{G}}_1(\bar{r}, \bar{r}') \cdot \overline{J}_1^{(n)}(\bar{r}') \right) \times \hat{n}_o(\bar{r}) = 0 \qquad \text{for } \bar{r} \in S_1, \tag{20}$$

$$\overline{E}_i^{(n)}(\bar{r}) + \iint_{S_o} d\bar{r}'_\perp \left\{ ik_1 \overline{\overline{G}}_1\left(\bar{r}, \bar{r}'_\perp\right) \cdot \bar{a}_\perp^{(n)}(\bar{r}'_\perp) + \nabla \times \overline{\overline{G}}_1\left(\bar{r}, \bar{r}'_\perp\right) \cdot \bar{b}_\perp^{(n)}(\bar{r}'_\perp) \right\} + i\omega\mu_1 \iint_{S_1} dS' \overline{\overline{G}}_1(\bar{r}, \bar{r}') \cdot \overline{J}_1^{(n)}(\bar{r}') = 0 \qquad \text{for } \bar{r} \in V_2, \tag{21}$$

$$\overline{E}_{i2}^{(n)}(\bar{r}) + \iint_{S_o} d\bar{r}'_\perp \left\{ ik_2 \frac{\eta_2}{\eta_1} \overline{\overline{G}}_2\left(\bar{r}, \bar{r}'_\perp\right) \cdot \bar{a}_\perp^{(n)}(\bar{r}'_\perp) + \nabla \times \overline{\overline{G}}_2(\bar{r}, \bar{r}'_\perp) \cdot \bar{b}_\perp^{(n)}(\bar{r}'_\perp) \right\} = 0 \qquad \text{for } \bar{r} \in V_1, \tag{22}$$

where for $n = 0$,

$$\overline{E}_i^{(0)}(\bar{r}) = \overline{E}_i(\bar{r}), \tag{23}$$

$$\overline{E}_{i2}^{(0)}(\bar{r}) = 0, \tag{24}$$

for $n \geq 1$,

$$\overline{E}_i^{(n)}(\bar{r}) = \sum_{m=1}^{n} \frac{1}{m!} \iint d\bar{r}'_\perp \left[-f(\bar{r}'_\perp)\right]^m$$

$$\frac{\partial^m}{\partial z^m}\Bigg\{ik_1\overline{\overline{G}}_1\left(\bar{r},\bar{r}'_\perp\right)\cdot\bar{a}_\perp^{(n-m)}(\bar{r}'_\perp)+\nabla\times\overline{\overline{G}}_1\left(\bar{r},\bar{r}'_\perp\right)\cdot\bar{b}_\perp^{(n-m)}(\bar{r}'_\perp)\Bigg\}$$
$$+\sum_{m=1}^{n}\frac{1}{(m-1)!}\iint d\bar{r}'_\perp\left[-f(\bar{r}'_\perp)\right]^{m-1}$$
$$\frac{\partial^{m-1}}{\partial z^{m-1}}\Bigg\{ik_1\overline{\overline{G}}_1\left(\bar{r},\bar{r}'_\perp\right)\cdot\hat{z}\left[\nabla'_\perp f(\bar{r}'_\perp)\cdot\bar{a}_\perp^{(n-m)}(\bar{r}'_\perp)\right]$$
$$+\nabla\times\overline{\overline{G}}_1\left(\bar{r},\bar{r}'_\perp\right)\cdot\hat{z}\left[\nabla'_\perp f(\bar{r}'_\perp)\cdot\bar{b}_\perp^{(n-m)}(\bar{r}'_\perp)\right]\Bigg\}, \tag{25}$$

$$\overline{E}_{i2}^{(n)}(\bar{r})=\sum_{m=1}^{n}\frac{1}{m!}\iint d\bar{r}'_\perp\left[-f(\bar{r}'_\perp)\right]^m$$
$$\frac{\partial^m}{\partial z^m}\Bigg\{\frac{ik_2\eta_2}{\eta_1}\overline{\overline{G}}_2\left(\bar{r},\bar{r}'_\perp\right)\cdot\bar{a}_\perp^{(n-m)}(\bar{r}'_\perp)+\nabla\times\overline{\overline{G}}_2(\bar{r},\bar{r}'_\perp)\cdot\bar{b}_\perp^{(n-m)}(\bar{r}'_\perp)\Bigg\}$$
$$+\sum_{m=1}^{n}\frac{1}{(m-1)!}\iint d\bar{r}'_\perp\left[-f(\bar{r}'_\perp)\right]^{m-1}$$
$$\frac{\partial^{m-1}}{\partial z^{m-1}}\Bigg\{ik_2\frac{\eta_2}{\eta_1}\overline{\overline{G}}_2\left(\bar{r},\bar{r}'_\perp\right)\cdot\hat{z}\left[\nabla'_\perp f(\bar{r}'_\perp)\cdot\bar{a}_\perp^{(n-m)}(\bar{r}'_\perp)\right]$$
$$+\nabla\times\overline{\overline{G}}_2(\bar{r},\bar{r}'_\perp)\cdot\hat{z}\left[\nabla'_\perp f(\bar{r}'_\perp)\cdot\bar{b}_\perp^{(n-m)}(\bar{r}'_\perp)\right]\Bigg\}. \tag{26}$$

Comparing the zeroth order ($n=0$) integral equations with Eqs. (6)–(8) for the flat interface ($f(\bar{r}'_\perp)=0$), we see that they are the same except adding a superscript (0) to the surface variables $\bar{a}_\perp$ and $\bar{b}_\perp$ and to the induced current $\overline{J}_1$. Therefore, the solutions $\bar{a}_\perp^{(0)}$, $\bar{b}_\perp^{(0)}$, and $\overline{J}_1^{(0)}$ for the zeroth order equations should be the same as the ones for Eqs. (6)–(8) in which the rough surface is considered to be flat. For the higher order equations ($n\geq 1$), we find that they are also in the same form as the zeroth order equations, except for the substitution of $\overline{E}_i$ by $\overline{E}_i^{(n)}$, and the additional "source" term $\overline{E}_{i2}^{(n)}$ in the lower region. Therefore we only need to know how to solve the zeroth order equations, i.e., the equations for an object over a flat interface.

Since the equations of any order are equivalent to the ones for a flat interface, they can be rewritten by introducing the dyadic Green's

function for layered media. The advantage of this approach is avoiding to solve surface unknowns $\bar{a}_{\perp}^{(n)}$ and $\bar{b}_{\perp}^{(n)}$ on the interface. Only the induced current $\overline{J}_1^{(n)}$ on the conducting body needs to be solved for. Therefore both the computational time and memory requirement can be dramatically reduced.

2.4 Application to Perfectly Conducting Rough Surface

As an example, we now consider the rough surface to be perfectly conducting. In this case the zeroth order electric field integral equation (EFIE) can be written as

$$\hat{n}_o(\bar{r}) \times \left(\overline{E}_i^{(0)}(\bar{r}) + \overline{E}_r^{(0)}(\bar{r}) + i\omega\mu_1 \int_{S_1} dS' \overline{\overline{G}}_L(\bar{r}, \bar{r}') \cdot \overline{J}_1^{(0)}(\bar{r}') \right) = 0 \qquad \text{for } \bar{r} \in S_1, \tag{27}$$

and the n-th order ($n \geq 1$) EFIE can be written as

$$\hat{n}_o(\bar{r}) \times \left(\overline{E}_i^{(n)}(\bar{r}) + \overline{E}_r^{(n)}(\bar{r}) + i\omega\mu_1 \int_{S_1} dS' \overline{\overline{G}}_L(\bar{r}, \bar{r}') \cdot \overline{J}_1^{(n)}(\bar{r}') \right) = 0 \qquad \text{for } \bar{r} \in S_1, \tag{28}$$

where

$$\begin{aligned} \overline{E}_i^{(n)}(\bar{r}) = & \sum_{m=1}^{n} \frac{1}{m!} \iint d\bar{r}'_{\perp} \left[-f(\bar{r}'_{\perp}) \right]^m \frac{\partial^m}{\partial z^m} \left\{ ik_1 \overline{\overline{G}}_1 \left(\bar{r}, \bar{r}'_{\perp} \right) \cdot \bar{a}_{\perp}^{(n-m)}(\bar{r}'_{\perp}) \right\} \\ & + \sum_{m=1}^{n} \frac{1}{(m-1)!} \iint d\bar{r}'_{\perp} \left[-f(\bar{r}'_{\perp}) \right]^{m-1} \\ & \frac{\partial^{m-1}}{\partial z^{m-1}} \left\{ ik_1 \overline{\overline{G}}_1 \left(\bar{r}, \bar{r}'_{\perp} \right) \cdot \hat{z} \left[\nabla'_{\perp} f(\bar{r}'_{\perp}) \cdot \bar{a}_{\perp}^{(n-m)}(\bar{r}'_{\perp}) \right] \right\}, \end{aligned} \tag{29}$$

and the dyadic Green's function for a perfectly conducting interface is

$$\overline{\overline{G}}_L(\bar{r}, \bar{r}') = \overline{\overline{G}}_1(\bar{r}, \bar{r}') - \overline{\overline{G}}_1(\bar{r}, (\overline{\overline{I}} - 2\hat{z}\hat{z}) \cdot \bar{r}') \cdot (\overline{\overline{I}} - 2\hat{z}\hat{z}), \tag{30}$$

where $\overline{\overline{G}}_1$ is the dyadic Green's function in the unbounded medium of region V_1. The singularities of the dyadic Green's functions in

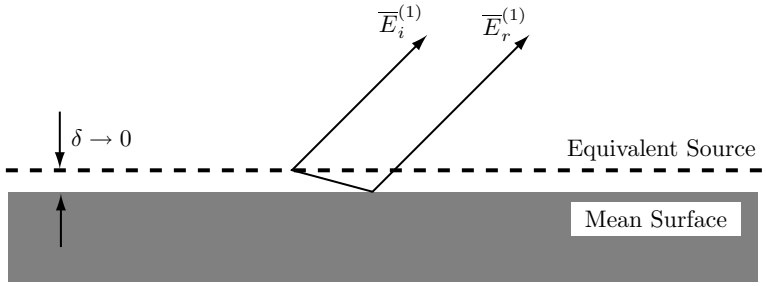

Figure 2. Radiation and reflection of the equivalent source.

Eqs. (27) and (28) can be reduced by using a triangular patch model in [18] for the conducting surface of the object.

The surface field $\bar{a}_\perp$ of lower order can be obtained from the lower order scattered field due to object and equivalent source. For example, the first order surface variable $\bar{a}_\perp^{(1)}$ can be calculated by using the solution of the zeroth order induced current $\overline{J}_1^{(0)}$ and the incident and reflected magnetic fields in absence of the object,

$$\bar{a}_\perp^{(0)}(\bar{r}'_\perp) = \eta_1 \hat{z} \times \left(\overline{H}_{i1}(\bar{r}'_\perp) + \overline{H}_{r1}(\bar{r}'_\perp) + \int_{S_1} dS'' \nabla' \times \overline{\overline{G}}_L(\bar{r}'_\perp, \bar{r}'') \cdot \overline{J}_1^{(0)}(\bar{r}'') \right). \tag{31}$$

The higher order ($n \geq 2$) surface variable $\bar{a}_\perp^{(n)}$ can be obtained similarly but involving much more manipulation.

Up to the first order, the total returned field can be written as

$$\overline{E}_s(\bar{r}) = \overline{E}_r(\bar{r}) + \overline{E}_b(\bar{r}) + \overline{E}_c(\bar{r}) + \overline{E}_d(\bar{r}), \tag{32}$$

where

$$\overline{E}_b(\bar{r}) = i\omega\mu_1 \int_{S_1} dS' \overline{\overline{G}}_L(\bar{r}, \bar{r}') \cdot \overline{J}_1^{(0)}(\bar{r}'), \tag{33}$$

$$\overline{E}_c(\bar{r}) = \overline{E}_i^{(1)}(\bar{r}) + \overline{E}_r^{(1)}(\bar{r}), \tag{34}$$

$$\overline{E}_d(\bar{r}) = i\omega\mu_1 \int_{S_1} dS' \overline{\overline{G}}_L(\bar{r}, \bar{r}') \cdot \overline{J}_1^{(1)}(\bar{r}'), \tag{35}$$

and

$$\overline{E}_i^{(1)}(\bar{r}) = -ik_1 \iint d\bar{r}'_\perp f(\bar{r}'_\perp) \frac{\partial}{\partial z} \overline{\overline{G}}_1 \left(\bar{r}, \bar{r}'_\perp\right) \cdot \bar{a}_\perp^{(0)}(\bar{r}'_\perp) + ik_1 \iint d\bar{r}'_\perp \overline{\overline{G}}_1 \left(\bar{r}, \bar{r}'_\perp\right) \cdot \hat{z} \left[\nabla'_\perp f(\bar{r}'_\perp) \cdot \bar{a}_\perp^{(0)}(\bar{r}'_\perp)\right]. \quad (36)$$

In Eq. (32), $\overline{E}_r(\bar{r})$ is simply the reflected field from the flat interface in absence of the conducting object. In the expression for $\overline{E}_b(\bar{r})$ [Eq. (33)], the induced current $\overline{J}_1^{(0)}$ is obtained by solving the integral equation (27) with layered Green's function, therefore the returned field $\overline{E}_b(\bar{r})$ includes all interactions between object and flat interface. $\overline{E}_c(\bar{r})$ in Eq. (34) is the sum of the radiated field from the "equivalent source" and its reflection, as illustrated in Fig. 2. The reflected field of the equivalent source can be obtained by writing the unbounded dyadic Green's function in integral form as in Appendix A, thus the radiated field of the equivalent source $\overline{E}_i^{(1)}$ is expressed as the sum of plane waves. By using the Fresnel reflection coefficient for each plane wave component, it is easy to write the reflected field $\overline{E}_r^{(1)}$ by multiplying with R^{TE} and R^{TM} to obtain the reflected TE and TM waves, respectively. For a perfectly conducting surface $R^{TE} = -1$ and $R^{TM} = 1$, thus we find

$$\overline{E}_r^{(1)}(\bar{r}) = \overline{E}_i^{(1)}(\bar{r}). \quad (37)$$

Therefore the return field due to the equivalent source is simply

$$\overline{E}_c(\bar{r}) = 2\overline{E}_i^{(1)}(\bar{r}). \quad (38)$$

It can also be shown that the returned field $\overline{E}_c(\bar{r})$ as in Eq. (38) is the same as the first order SPM solution for a conducting rough surface if we let the induced current $\overline{J}_1^{(0)} = 0$ when evaluating the surface field $\bar{a}_\perp^{(0)}(\bar{r}'_\perp)$ in Eq. (31). Therefore, we call the return field $\overline{E}_c(\bar{r})$ the "incoherent" returned field from the rough surface under the influence of the object. The returned field $\overline{E}_d(\bar{r})$ is the radiated field of the first order induced current $\overline{J}_1^{(1)}$ excited by the "incoherent" field $\overline{E}_c(\bar{r})$. Since the layered Green's function is used to calculate the induced current $\overline{J}_1^{(1)}$ and its radiated field, the returned field $\overline{E}_d(\bar{r})$ includes all multiple interactions between the object and the conducting interface.

3. NUMERICAL RESULTS

In the numerical simulation, a horizontal conducting cylinder along the x-axis with $2.0\,\lambda$ in length and $1.0\,\lambda$ in diameter is considered. The distance between the bottom of the cylinder and the mean surface height of the conducting rough surface is $0.1\,\lambda$ so that strong interaction between object and rough surface can be expected. A rough surface with the well-known Gaussian power spectrum is used for the validation with the help of the standard method of moments (MoM). The size of the rough surface is $15.0\,\lambda$ by $15.0\,\lambda$. The deviation and correlation length of the rough surface are $\sigma = 0.03\lambda$ and l=$1.0\,\lambda$, respectively. The incident wave $\overline{E}_i$ is tapered and formed as a summation of plane waves with Gaussian-shaped footprint on the mean surface. This tapered incident wave satisfies Maxwell's equations and minimizes the edge effect in the numerical calculations. The factor g, which is used to control the beam width of the tapered wave is $g = 3.0\lambda$, so that the incident electric field magnitude on the rough surface has dropped by a factor of $1/e$ at $|\bar{r}'_\perp| = 3.0\lambda$.

In the numerical calculation, the radar cross section (RCS) is defined as

$$\mathrm{RCS} = \lim_{r\to\infty} 4\pi r^2 \frac{|E_s(\theta,\phi)|^2}{|E_o(\theta_i,\phi_i)|^2}, \tag{39}$$

where E_o is the maximum magnitude of the tapered incident electric field on the mean surface S_o. For monostatic (backscattering) RCS, the scattering angles are $\theta = \theta_i$ and $\phi = \phi_i$. In the numerical simulations for bistatic RCS, we let the polar angle θ be 40° and vary the azimuthal angle ϕ from 0° to 360°. $\phi = 0^\circ$ is the backscattering direction. For the monostatic RCS simulations, the incident $\bar{k}_i$ vector remains in the xz-plane and the incident angle θ_i varies from 0° to 90°.

The plots shown in Fig. 3 and Fig. 4 are bistatic RCSs for the individual terms of Eq. (32) for TE and TM incident waves, respectively. The plot labeled as E_r is the reflected field of the incident tapered wave from the flat interface in absence of the object. A peak of copolarized component of $\overline{E}_r$ appears in the specular direction $\phi = 180^\circ$ as expected. The plot labeled as E_b is the returned field as in Eq. (33). The E_c plot is evaluated by using Eq. (34), and the E_d plot is calculated from Eq. (35). It can be seen that most of the energy of the "incoherent" field $\overline{E}_c$ concentrates in the forward scattering direction. The curves shown in the E_b plot represent the scattering from the ob-

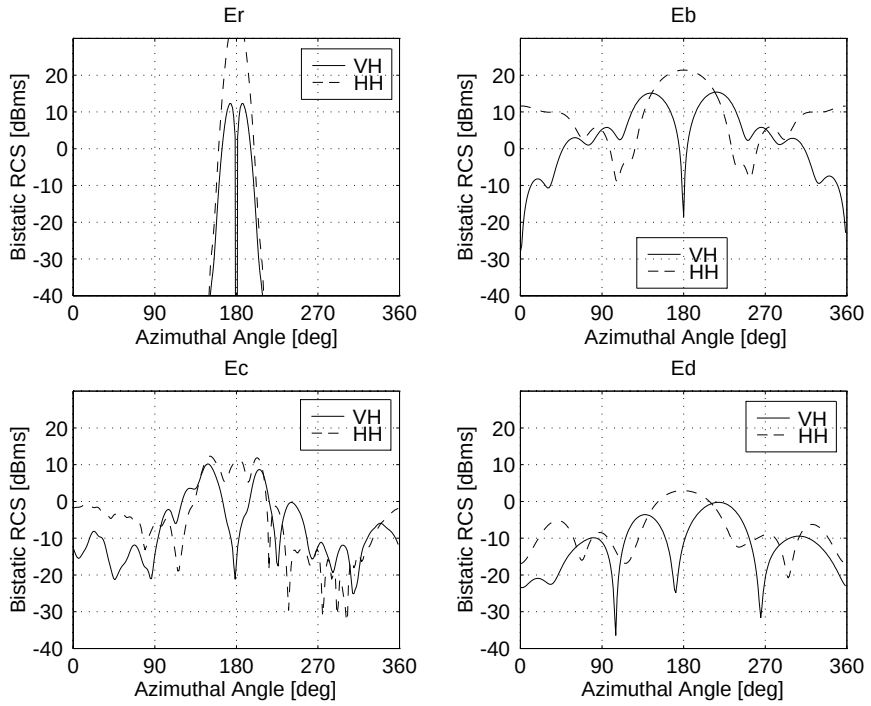

Figure 3. Bistatic RCS of individual terms for TE incident wave.

ject excited by the fields $\overline{E}_i$ and $\overline{E}_r$, while the secondary scattering field in the E_d plot is the returned field from the object excited by the "incoherent" field $\overline{E}_c$ from the rough surface. We note that the cross-polarized returns VH and HV in the backscattering direction are zero in the E_b plot. This is due to the symmetry of the geometry and the incident wave. The secondary returned fields of cross-polarized VH and HV in the plot labeled E_d are no longer zero in the backscattering direction due to the asymmetry of the "incoherent" field $\overline{E}_c$. The "incoherent" field $\overline{E}_c$ as well as the secondary returned field $\overline{E}_d$ from the object are both proportional to the surface height function $f(\bar{r}'_\perp)$ of the rough surface. It can be easily checked that both $\overline{E}_c$ and $\overline{E}_d$ become zero when the surface height function is zero.

The sum of the four terms $\overline{E}_r + \overline{E}_b + \overline{E}_c + \overline{E}_d$ as in Eq. (32) is the total returned field up to the first order, and the corresponding RCS are shown in Fig. 5 and Fig. 6 for TE and TM incident wave, respectively. The bistatic RCS for the total returned field are compared with

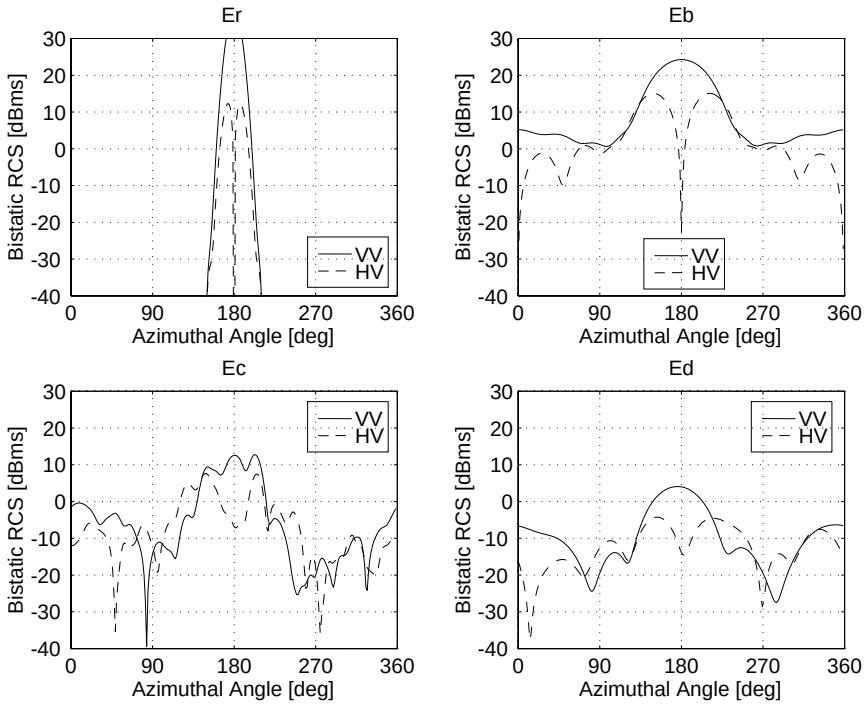

Figure 4. Bistatic RCS of individual terms for TM incident wave.

standard MoM results. In the MoM simulation, both the rough surface and the conducting object are discretized and the surface unknowns are solved together by using the conjugate gradient algorithm. The plots in the top rows of Fig. 5 and Fig. 6 show the bistatic RCS of the zeroth order solution using the hybrid technique and the standard MoM solution. Good agreement is found comparing the results. The co-polarized VV of the zeroth order solution matches better than the co-polarized HH, since the TE incident wave may induce significant currents on the front and back edges of the rough surface, which may give more return for the MoM result. This edge effect can be minimized if the TM incident wave is used (Fig. 6). In the simulations as shown in the bottom rows of Fig. 5 and Fig. 6, a single rough surface with Gaussian power spectrum is used. The deviation of the surface height is $\sigma = 0.03\lambda$ and the correlation length is $l = 1.0\lambda$. Again the results show good agreement comparing the hybrid technique with the standard MoM. It is noted that the curves are no longer symmetrical

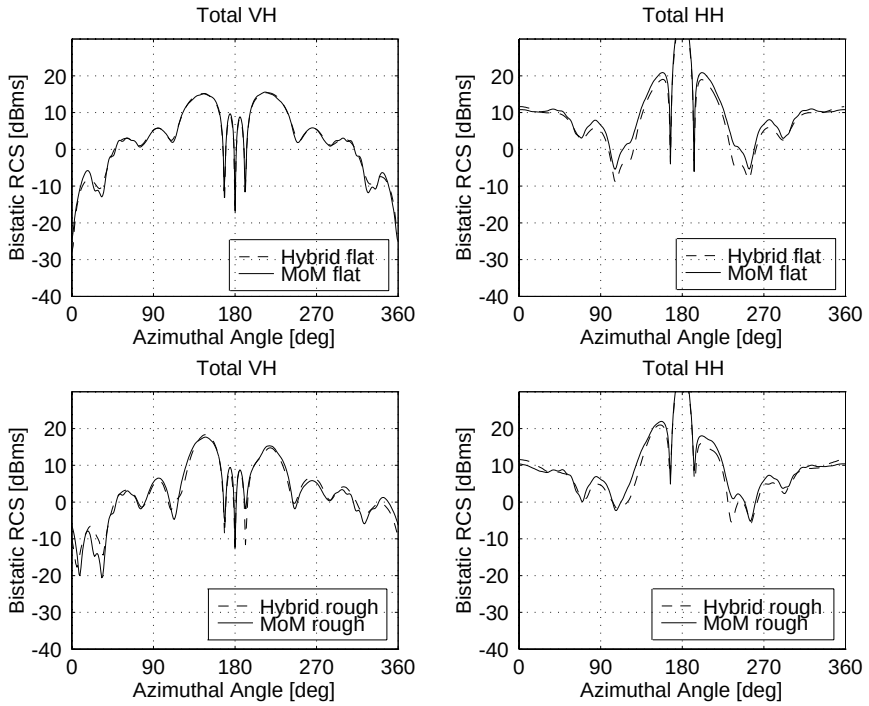

Figure 5. Bistatic RCS of the total returned field $\overline{E}_r + \overline{E}_b + \overline{E}_c + \overline{E}_d$ for TE incident wave.

with respect to the plane of incidence when the surface is rough.

Monte Carlo simulation results with 100 realizations are shown in Fig. 7 and Fig. 8 for TE and TM incident waves, respectively. Rough surfaces with power law spectrum are generated and they are statistically independent of each other. The power law spectrum is $W(k) = a_o/k^4$, which more closely represents ocean surfaces than the Gaussian power spectrum. Here k is the spatial wavenumber of the rough surface and $a_o = 0.008/2\pi$ which is the amplitude used for the Durden-Vesecky spectrum [32]. The upper cut-off spatial wavenumber k_h is chosen to be $k_h = 2.5k_1$ which corresponds to the band width for $1/5\lambda_1$ spatial resolution of sampling on the rough surface, where k_1 and λ_1 are electromagnetic wavenumber and wavelength of the incident wave, respectively. The lower cut-off spatial wavenumber k_l is chosen according to the standard deviation of the rough surface height

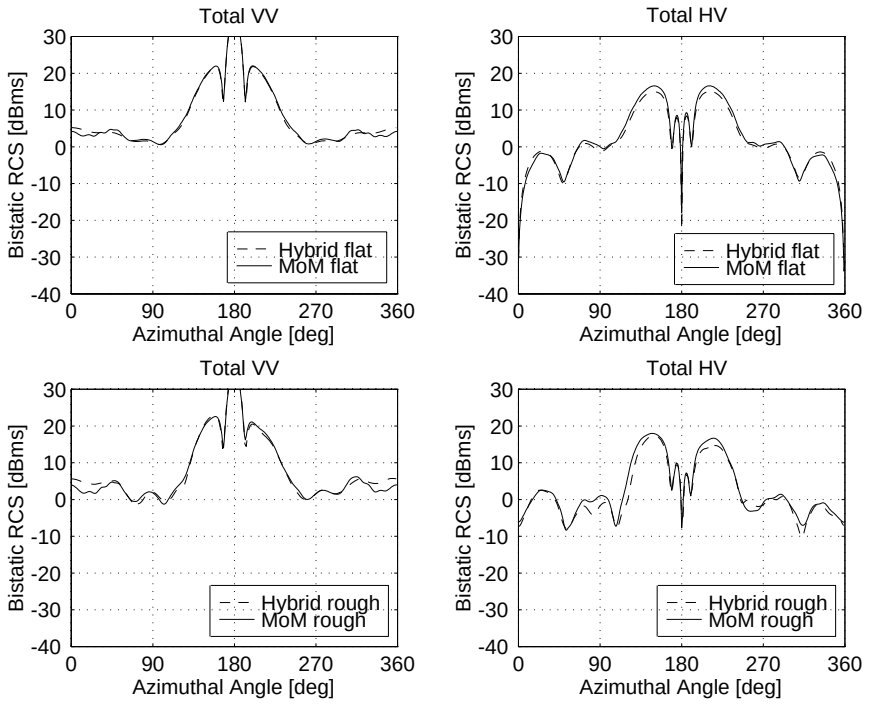

Figure 6. Bistatic RCS of the total returned field $\overline{E}_r + \overline{E}_b + \overline{E}_c + \overline{E}_d$ for TM incident wave.

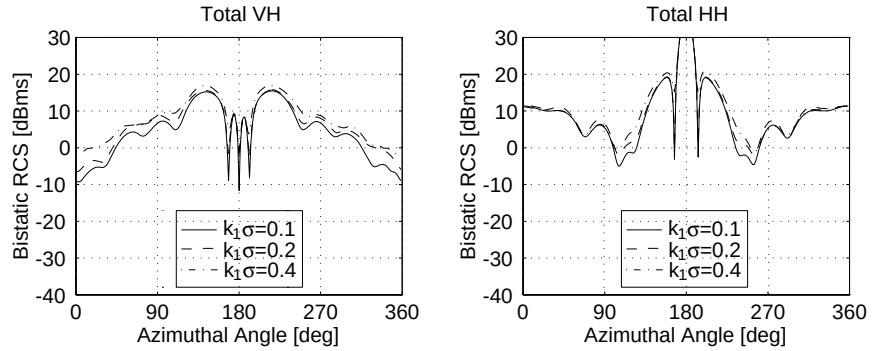

Figure 7. Monte Carlo simulation of bistatic RCS of the total returned field $\overline{E}_r + \overline{E}_b + \overline{E}_c + \overline{E}_d$ for TE incident wave.

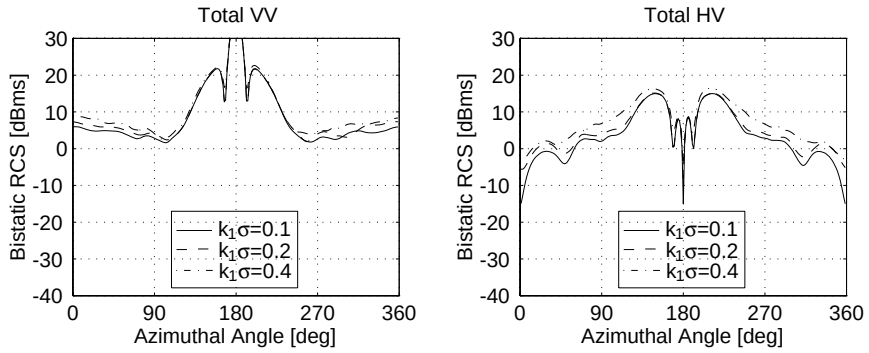

Figure 8. Monte Carlo simulation of bistatic RCS of the total returned field $\overline{E}_r + \overline{E}_b + \overline{E}_c + \overline{E}_d$ for TM incident wave.

using the following relation:

$$\sigma^2 = \int W(k) d^2k = \pi a_o \left(\frac{1}{k_l^2} - \frac{1}{k_h^2} \right). \tag{40}$$

In Fig. 7 and Fig. 8, the deviations of the rough surface $k_1\sigma = 0.1,\ 0.2,\ 0.4$ correspond to the lower cut-off spatial wavenumbers $k_l/k_1 = 0.6131,\ 0.3137,\ 0.1578$, respectively. It is noted that the Monte Carlo simulations converge with respect to the number of realizations. The averaged cross-polarized RCS increases with the deviation of the rough surface over a wide range of scattering angles.

Fig. 9 and Fig. 10 show the Monte Carlo simulation of monostatic (backscattering) RCS for TE and TM incident waves, respectively. Here 100 rough surfaces with power law spectrum and $k_1\sigma = 0.4$ are used. The backscattering direction varies from $\theta = 0^\circ$ to $\theta = 90^\circ$ with 45 steps in between. The azimuthal angle ϕ remains 0 degree. We note that the cross-polarized VH and HV are significant in the presence of a rough surface. Analytically the cross-polarized returns should be zero for the considered geometry when the surface is flat. We note that the non-zero values for flat surface are produced numerically. Changes of co-polarized monostatic RCS due to the rough surface can be found at some scattering angles. At small grazing angles, the rough surface effect on co-polarized backscattering RCS is not significant. In the standard MoM, the number of unknowns is 17,252 with the sampling resolution being $1/5\lambda$ on the rough surface and the object. In

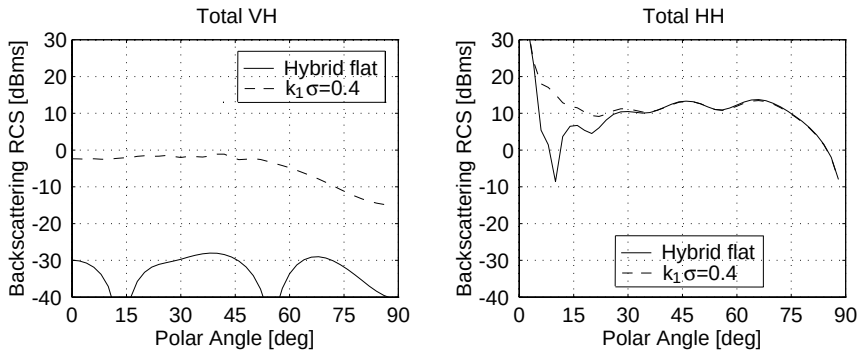

Figure 9. Monte Carlo simulation of monostatic RCS of the total returned field $\overline{E}_r + \overline{E}_b + \overline{E}_c + \overline{E}_d$ for TE incident wave.

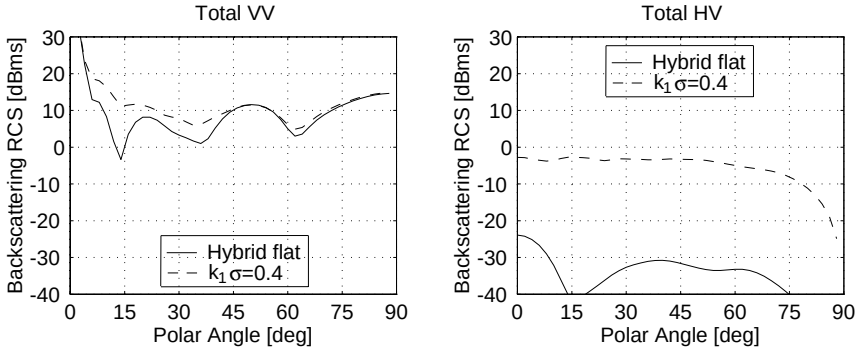

Figure 10. Monte Carlo simulation of monostatic RCS of the total returned field $\overline{E}_r + \overline{E}_b + \overline{E}_c + \overline{E}_d$ for TM incident wave.

the hybrid technique, the number of unknowns is only 972 with the same sampling resolution on the object. There is no need to solve for surface unknowns on the rough surface using the hybrid technique.

4. CONCLUSION

This paper presents a hybrid technique of SPM and MoM for EM scattering from an object above rough surface. With the expansion of the Green's function and surface variables in terms of the surface height function on the flat mean surface, the electric field integral equations are decomposed into different orders. The equations of each order represent the EM scattering problem with the same object above the mean

surface and different incident field from an equivalent source which can be evaluated by using lower order solutions. The equivalence with a flat surface problem allows us to use the dyadic Green's function for layered media, so that we do not need to solve for tangential fields on the rough surface, leaving only unknowns on the conducting object. The number of unknowns in the hybrid method is about 20 times less than in the standard MoM. Therefore this hybrid technique demonstrates a dramatic increase in computational efficiency without losing accuracy. The separation of the return field into the sum of individual interaction terms allows us to identify the coherent and incoherent returned field, and thus to characterize the rough surface effects quantitatively.

ACKNOWLEDGMENT

This work was supported by ONR Grant N00014-97-I-017, ONR Grant N00014-92-J-4098, and Lincoln Agreement CX-21854. The first author would like to thank C. Ao from the MIT physics department for the insightful discussion of SPM.

APPENDIX A.

The integral representation of the dyadic Green's function in unbounded space is given by [31]

$$\overline{\overline{G}}_1(\bar{r},\bar{r}') = -\hat{z}\hat{z}\frac{\delta(\bar{r},\bar{r}')}{k_1^2} + \begin{cases} \dfrac{i}{8\pi^2}\displaystyle\iint dk_x dk_y \frac{1}{k_{1z}}\left[\hat{e}(k_{1z})\hat{e}(k_{1z}) + \hat{h}(k_{1z})\hat{h}(k_{1z})\right] e^{i\bar{k}_1\cdot(\bar{r}-\bar{r}')} & z > z', \\ \dfrac{i}{8\pi^2}\displaystyle\iint dk_x dk_y \frac{1}{k_{1z}}\left[\hat{e}(-k_{1z})\hat{e}(-k_{1z}) + \hat{h}(-k_{1z})\hat{h}(-k_{1z})\right] e^{i\overline{K}_1\cdot(\bar{r}-\bar{r}')} & z < z', \end{cases} \tag{41}$$

where

$$\hat{e}(\pm k_{1z}) = \frac{\hat{x}k_y - \hat{y}k_x}{\sqrt{k_x^2 + k_y^2}}, \tag{42}$$

$$\hat{h}(\pm k_{1z}) = \mp\frac{k_{1z}}{k_1\sqrt{k_x^2 + k_y^2}}(\hat{x}k_x + \hat{y}k_y) + \hat{z}\frac{\sqrt{k_x^2 + k_y^2}}{k_1}, \tag{43}$$

$$\bar{k}_1 = k_x\hat{x} + k_y\hat{y} + k_{1z}\hat{z}, \tag{44}$$

$$\overline{K}_1 = k_x\hat{x} + k_y\hat{y} - k_{1z}\hat{z}, \tag{45}$$

$$k_{1z} = \sqrt{k_1^2 - k_x^2 - k_y^2}. \tag{46}$$

REFERENCES

1. Dogaru, T., L. Carlin, B. L. Merchant, and C. F. Lee, "Electromagnetic scattering and detection of mines near a rough air-ground interface," *Proc. SPIE-Int. Soc. Opt. Eng. (USA),* Vol. 3079, 704–715, April 1997.
2. Kang, J. S. and W. C. Chew, "Time-domain distorted Born iterative method for imaging buried dielectric cylinder in underground lossy media," *IEEE Antennas and Propagat. Soc. Int'l. Symp. 1996 Digest,* Vol. 3, 2156–2159, 1996.
3. Daniels, D. J., "Surface-penetrating radar," *Electron. & Comm. Eng. J.,* Vol. 8, No. 4, 165–182, Aug. 1996.
4. O'Neill, K., R. F. Lussky, Jr., and K. D. Paulsen, "Scattering from a metallic object embedded near the randomly rough surface of a lossy dielectric," *IEEE Trans. Geosci. Remote Sens.,* Vol. 34, No. 2, 367–376, Mar. 1996.
5. Helaly, A., A. Sebak, and L. Shafai, "Scattering by a buried conducting object of general shape at low frequencies," *IEE Proc. H (Microwaves, Antennas and Propagat.),* Vol. 138, No. 3, 213–218, June 1991.
6. Tajima, K. and S.-I. Iiguchi, "Analysis of electromagnetic wave scattered from cylinders buried in the ground," *Electron. Comm. Japan,* Part 1 (Communications), Vol. 70, No. 5, 86–94, May 1987.
7. Cottis, P. G. and J. D. Kanellopoulos, "Scattering from a conducting cylinder above a lossy medium," *Int'l J. Electron.,* Vol. 65, No. 5, 1031–1038, Nov. 1988.
8. Richmond, J. H., "A wire-grid model for scattering by conducting bodies," *IEEE Trans. Antennas Propagat.,* Vol. AP-14, No. 6, 782–786, Nov. 1966.
9. Miller, E. K. and F. J. Deadrick, "Some computational aspects of thin-wire modeling," in *Numerical and Asymptotic Techniques in Electromagnetics,* R. Mittra, Ed., Ch. 4, Springer-Verlag, New York, 1975.
10. Lee, K. S. H., L. Marin, and J. P. Castillo, "Limitations of wire-grid modeling of a closed surface," *IEEE Trans. Electromagn. Compat.,* Vol. EMC-18, No. 3, 123–129, Aug. 1976.

11. Knepp, D. L. and J. Goldhirsh, "Numerical analysis of electromagnetic radiation properties of smooth conducting bodies of arbitrary shape," *IEEE Trans. Antennas Propagat.,* Vol. AP-20, No. 3, 383–388, May 1972.
12. Albertsen, N. C., J. E. Hansen, and N. E. Jensen, "Computation of radiation from wire antennas on conducting bodies," *IEEE Trans. Antennas Propagat.,* Vol. AP-22, No. 2, 200–206, Mar. 1974.
13. Wang, N. N., J. H. Richmond, and M. C. Gilreath, "Simusoidal reaction formulation for radiation and scattering from conducting surfaces," *IEEE Trans. Antennas Propagat.,* Vol. AP-23, No. 3, 376–382, May 1975.
14. Newman, E. H. and D. M. Pozar, "Electromagnetic modeling of composite wire and surface geometries," *IEEE Trans. Antennas Propagat.,* Vol. AP-26, No. 6, 784–789, Nov. 1978.
15. Sankar, A. and T. C. Tong, "Current computation on complex structures by finite element method," *Electron. Lett.,* Vol. 11, No. 20, 481–482, Oct. 1975.
16. Wang, J. J. H., "Numerical analysis of three-dimensional arbitrarily-shaped conducting scatterers by trilateral surface cell modeling," *Radio Sci.,* Vol. 13, No. 6, 947–952, Nov.-Dec. 1978.
17. Singh, J. and A. T. Adams, "A non-rectangular patch model for scattering from surfaces," *IEEE Trans. Antennas Propagat.,* Vol. AP-27, No. 4, 531–535, July 1979.
18. Rao, S. M., D. R. Wilton, and A. W. Glisson, "Electromagnetic scattering by surfaces of arbitrary shape," *IEEE Trans. Antennas Propagat.,* Vol. AP-30, No. 3, 409–418, May 1982.
19. Parry, J. R. and S. H. Ward "Electromagnetic scattering from cylinders of arbitrary cross-section in a conductive half-space," *Geophysics,* Vol. 36, No. 1, 67–100, Feb. 1971.
20. Howard, A. Q., "The electromagnetic fields of a subterranean cylindrical inhomogeneity excited by a line source," *Geophysics,* Vol. 37, No. 6, 975–984, Dec. 1972.
21. Mahmoud, S. F., S. M. Ali, and J. R. Wait, "Electromagnetic scattering from a buried cylindrical inhomogeneity inside a lossy earth," *Radio Sci.,* Vol. 16, No. 6, 1285–1298, Nov.-Dec. 1981.
22. Butler, C. M., "Current induced on a conducting strip which resides on the planar interface between two semi-infinite half-spaces," *IEEE Trans. Antennas Propagat.,* Vol. AP-32, No. 3, 226–231, Mar. 1984.
23. Butler, C. M., X. B. Xu, and A. W. Glisson, "Current induced on a conducting cylinder located near the planar interface between two semi-infinite half-spaces," *IEEE Trans. Antennas Propagat.,*

Vol. AP-33, No. 6, 616–624, June 1985.

24. Xu, X. B. and C. M. Butler, "Current induced by TE excitation on a conducting cylinder located near the planar interface between two semi-infinite half-spaces," *IEEE Trans. Antennas Propagat.,* Vol. AP-34, No. 7, 880–890, July 1986.
25. Xu, X. B. and C. M. Butler, "Scattering of TM excitation by coupled and partially buried cylinders at the interface between two media," *IEEE Trans. Antennas Propagat.,* Vol. AP-35, No. 5, 529–538, May 1987.
26. Michalski, K. A. and D. Zheng, "Electromagnetic scattering and radiation by surfaces of arbitrary shape in layered media. I. Theory," *IEEE Trans. Antennas Propagat.,* Vol. 38, No. 3, 335–344, Mar. 1990.
27. Michalski, K. A. and D. Zheng, "Electromagnetic scattering and radiation by surfaces of arbitrary shape in layered media. II. Implementation and results for contiguous half-spaces," *IEEE Trans. Antennas Propagat.,* Vol. 38, No. 3, 345–352, Mar. 1990.
28. Ripoll, J., A. Madrazo, and M. Nieto-Vesperinas, "Scattering of electromagnetic waves from a body over a random rough surface," *Optics Communications,* Vol. 142, No. 4–6, 173–178, Oct. 1997.
29. Cui, T. J., W. Wiesbeck, and A. Herschlein, "Electromagnetic scattering by multiple three-dimensional scatterers buried under multilayered media. I. Theory," *IEEE Trans. Geosci. Remote Sens.,* Vol. 36, No. 2, 526–534, Mar. 1998.
30. Cui, T. J., W. Wiesbeck, and A. Herschlein, "Electromagnetic scattering by multiple three-dimensional scatterers buried under multilayered media. II. Numerical," *IEEE Trans. Geosci. Remote Sens.,* Vol. 36, No. 2, 535–546, Mar. 1998.
31. Kong, J. A., *Electromagnetic Wave Theory,* 2nd ed., John Wiley & Sons, New York, 1990.
32. Durden, S. P. and J. F. Vesecky, "A physical radar cross-section model for a wind-driven sea with swell," *IEEE J. Oceanic Eng.,* Vol. 10, 445–451, 1985.